JOURNAL OF MATERIALS SCIENCE 10 (1975) 243–251

Segregation of solutes in Al-Ni and Al-Sn alloys and its influence on their mechanical properties

A. BONEFAČIĆ, M. KERENOVIĆ, A. KIRIN, D. KUNSTELJ
Institute of Physics of the University of Zagreb, Yugoslavia

A study was made of the intensity of scattering of monochromatic X-rays at small angles from Al–3.6 at.% Ni and Al–0.26 at.% Sn solid solutions, in order to determine if the solutes are really dispersed. Electron-microscopic examinations were also carried out. Both alloys were obtained by rapid quenching from the melt in order to obtain the optimum dissolution. However, perfectly homogeneous solid solutions were not obtained, but agglomerations of solute atoms were detected. The evolution of clusters during annealing was examined. Their influence on microhardness and microstrain properties is discussed.

1. Introduction

One of the main purposes in studies of precipitation from supersaturated solid solution is to detect the initial progress of decomposition. In alloys quenched from the liquid state (splat cooling), supersaturation is achieved by rapidly cooling the system from the single phase liquid region, the faster the quench, the less clustered will be the solid solutions [1]. However, even the splat-cooling technique sometimes produces a fine dispersion of dissolved atoms in small clusters. Fontaine *et al.* [2] for instance, found that Al-3 at. % Fe samples quenched from the melt are not homogenous solid solutions but contian clusters which deform the aluminium matrix. Dartyge *et al.* [3] studying Al–Mn, Al–Ni and Al–Zn alloys, found that in all these alloys an ideally disordered solid solution cannot be obtained: in certain alloys (Al–Zn, Al–Mn) there was only a tendency to segregation, while in others (Al–Ni), there always existed clusters of dissolved atoms.

The structural transitions and the mechanical properties during the transformations of Al–3.6 at. % Ni and Al–0.26 at. % Sn solid solutions into the equilibrium phases have also been studied [4-6]. Since substantial hardening effects were observed in both Al–3.6 at. % Ni and Al–0.26 at. % Sn alloys quenched from the melt, and since the molten Al–Sn alloys, at higher Sn concentrations (15-20 at. %) have been interpreted as showing a "microheterogeneous" structure at temperatures above the liquidus [7], inhomogenities may also be expected in these solid solutions. Thus it was decided to study the Al–3.6 at. % Ni and Al–0.26 at. % Sn alloy in both as-quenched and annealed state, with regard to the absolute intensity of X-ray small-angle scattering and its change during annealing, in order to obtain more information on the nature of metastable structures in aluminium alloys quenched from the melt. Corresponding electron-microscopic examinations of the precipitate formation were also carried out. The results of these studies are compared with the measurements of microhardness [4] and microstrains [6] made earlier on the same alloys.

2. Experimental procedures

Alloys of Al–3.6 at. % Ni and Al–0.26 at. % Sn were prepared in an induction furnace at a pressure of 2×10^{-5} mm Hg and a temperature of about 750°C. The alloys were then rapidly quenched from the melt by the "two-piston" method to obtain supersaturated solid solutions. Details of the quenching have been described before [8]. The resulting quenched flakes were approximately circular (about 1 to 5 mm in diameter) and from 10 to 20 μm in thickness.

Absolute intensity measurements of the small-angle X-ray scattering were carried out with a Levelut-Guinier camera [9, 10] in which the primary beam is reflected on a doubly bent crystal and the monochromatic radiation (λ =

1.54 Å) is scattered on the specimen. After passing through the ring-shaped aperture the scattered radiation falls on the scintillation counter which detects its intensity. In changing the position of the aperture, one can detect the variation of intensity as the scattering angle changes. The measurements of the "absolute intensity", i.e. the determination of the scattered intensity relative to the primary beam energy, were carried out using a defined attenuation of the primary beam by an exact calibration of the set of copper filters. The absorption of the filters was carefully measured. For an absorption of the order of 10^5, we estimate that the error of measurement of the incident beam is about 5%.

The absolute intensities $I(s)$ were evaluated from the relation

$$I(s) = \frac{E(s)}{N \,.\, I_e \,.\, E_0 \,.\, d \,.\, \mathrm{d}\omega} \qquad (1)$$

where $E(s)$ is the energy of X-rays scattered in the solid angle $\mathrm{d}\omega$, $s = 2 \sin \theta/\lambda$, 2θ is the scattering angle, N the number of atoms in the unit volume, d the thickness of the sample, $I_e = 7.9 \times 10^{-26}$ cm^2 per electron, and E_0 is energy of the incident beam.

The measured intensities include thermal, Compton and double Bragg scatterings. These intensities may be calculated theoretically, using the formulae given by Warren and Walker [11-13], but these calculations are only approximate. Using the same technique we measured also the scattering of pure aluminium samples quenched from the melt, and subtracted it from the scattering given by Al–Ni and Al–Sn samples. In this way we could eliminate the contributions of the scattering due to the quenched-in vacancies or clusters of vacancies which were observed in splat-cooled aluminium samples [3].

3. Calculation of the scattered intensity

If dilute atoms in the matrix are distributed at random, the scattered intensity is spread uniformly over the entire volume in the reciprocal space. This Laue monotonic scattering [14] is given by

$$I = c_A c_B (f_A - f_B)^2 \qquad (2)$$

where c_A and c_B are atomic concentrations, and f_A and f_B the scattering factors. The absolute intensity I may be expressed as the scattering power per atom, i.e. the ratio of the scattered intensity per atom of the sample to the intensity scattered by a free electron in the same experimental conditions. If the substituted atoms are in small proportion, $c_A \approx 1$, $c_B \approx c$, and

$$I = c(f_A - f_B)^2 \,. \qquad (3)$$

The influence of lattice distortion, produced by dissolved atoms on the scattered intensity, may be expressed by an additional factor, and then Equation 3 becomes

$$I = c(f_A - f_B)^2 \left(1 - \frac{V_0 - V}{cV_0} \cdot \frac{f_A}{f_A - f_B}\right)^2 \qquad (4)$$

where V_0 and V are the atomic volumes of the solvent and solute atoms, respectively [10].

Equations 2 to 4 show that in the case of ideal solid solution the scattering decreases slowly with increasing scattering angles, the decrease being due to the monotonous variation of the scattering factor. However, ideal solid solution, with a perfectly random distribution of atoms, is rather an exception. A more realistic interpretation of scattering would be obtained by calculating the diffuse scattering from the coefficients of the short-range order α_m [14]. For the mth shell of neighbours in the case of binary solid solution

$$\alpha_m = 1 - \frac{n_{BA}}{c_A} \,,$$

n_{BA} being the proportion of pairs of BA atoms, and c_A the atomic concentration of A atoms. If the solution is completely disordered $\alpha_m = 0$; if there is a tendency towards clustering of B atoms $\alpha_m > 0$; and in the case of an ordering tendency $\alpha_m < 0$. The scattering influenced by short range order coefficients is given by [15]

$$I(s) = c_A c_B (f_A - f_B)^2 \sum_{m=0}^{\infty} c_m \alpha_m \frac{\sin 2\pi \mathbf{s}\mathbf{r}_m}{2\pi \mathbf{s}\mathbf{r}_m} \qquad (5)$$

where c_m is the number of neighbours situated at the distance $\mathbf{r}_m$ with respect to the given atom. When the scattering vector $\mathbf{s}$ is tending to 0, the ratio $\sin 2\pi \mathbf{s}\mathbf{r}_m / 2\pi \mathbf{s}\mathbf{r}_m$ tends to 1, and thus for small angles Equation 5 becomes [10]

$$I(0) = c_A c_B (f_A - f_B)^2 \sum_{m=0}^{\infty} c_m \alpha_m \,. \qquad (6)$$

For solid solution of low concentration c, a simple model of widely separated and very small agglomerations, each agglomeration including p dissolved atoms, may be considered. In this case the scattering is almost constant in the range of $2\theta = 2\text{-}6°$ and $\sum_m c_m \alpha_m = p$, i.e. intensity is p

times higher than the theoretical Laue scattering and given by

$$I(0) = pc(f_A - f_B)^2 . \quad (7)$$

However, in the case of a formation of clusters of solute atoms with dimensions higher than approximately 5 Å the scattering is not independent of angle, Equation 7 is no longer valid, and scattered intensities decrease with increasing scattering angle. The scattered intensities then depend on the shape and size of clusters and their electron density. In the case of certain standard particle shapes the scattered intensity as a function of angle can be calculated [16]. According to Porod's approximation [17] for the wings of the small-angle X-ray scattering intensity curve, the asymptotic value of intensity is given by

$$I = \frac{(\rho - \rho_0)^2}{8\pi^3} \frac{S}{s^4} \quad (8)$$

where ρ and ρ_0 are the density of particles and density of a medium respectively, and S is the total surface of the particles per unit mass. When s is not too small, the curve of log $I(s)$ versus log s are straight lines of slope -4, and the scattered intensity is proportional to the total surface of the particles contained in the unit mass.

4. Results and discussion

4.1. Al–3.6 at. % Ni samples quenched from the melt

Scattering intensities measured on the Al–3.6 at. % Ni alloy, after subtracting the scattering obtained with pure aluminium samples, are given in Table I. Fig. 1 presents the scattered intensity measured for as-quenched Al–3.6 at. % Ni alloy and the intensity of scattering after annealing the same sample at a temperature of 300°C.

In the case of a statistical distribution of Ni atoms, at the concentration of 3.6 at. % Ni, the intensity of the Laue scattering given by Equation 2 would be about 8 el/at for all the measured angles. In Fig. 1 the intensity of scattering decreases rapidly with increasing scattering angle indicating the existence of agglomerations of Ni atoms in the alloy. According to Equation 8 the intensity of scattered rays, in the case of the two-phase system, diminishes at large angles proportionally to s^{-4} and in the log $I(s)$ versus log s presentation a straight line with a constant slope should be obtained. Fig. 2 shows the logarithm of intensity as a function of logarithm

TABLE I

$s \times 10^2$ Å^{-1}	$I(s)$ electrons per atom				
	20°C	100°C	200°C	300°C	400°C
2.0	254.0	269.4	246.9	122.6	54.6
2.5	111.5	116.3	100.4	55.7	34.2
3.0	53.6	59.5	53.5	30.1	19.5
3.5	29.2	33.5	31.3	16.5	10.1
4.0	19.4	21.9	20.6	9.5	6.6
4.5	11.4	15.4	12.3	6.2	4.6
5.0	10.5	11.5	10.9	5.3	4.4
5.5	7.4	7.2	7.0	4.5	2.1
6.0	5.3	7.2	6.7	2.9	3.0
6.5	4.8	5.7	5.1	2.2	1.8
7.0	3.8	5.1	4.9	1.5	1.6
7.5	3.0	4.5	4.0	1.4	1.3
8.5	2.6	3.6	3.2	1.1	0.8
9.5	2.0	2.4	2.0	1.0	1.0

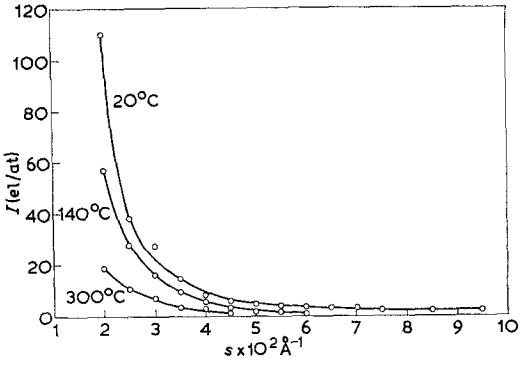

Figure 1 Scattered intensity measured for as-quenched (20°C) Al–3.6 at. % Ni alloy before and after annealing for 10 min at 300°C. Values of intensities are given after subtracting the corresponding scattering obtained with pure aluminium sample.

s in the case of the Al–3.6 at. % Ni system. A nearly straight line course with a slope of approximately -4 was obtained, which indicates that Porod's law may be used. Yet Porod's law is valid only when two phases are separated by a sharp boundary, which need not be fulfilled if precipitates are present.

Supposing two rough approximations – first that the agglomerations are spherical and secondly that the electron density of agglomerates is the same as that of the equilibrium precipitate Al_3Ni – we obtained a radius of agglomerates of 40 Å for as-quenched samples and 90 Å for samples annealed for 10 min at 300°C.

During annealing, the intensity of scattered

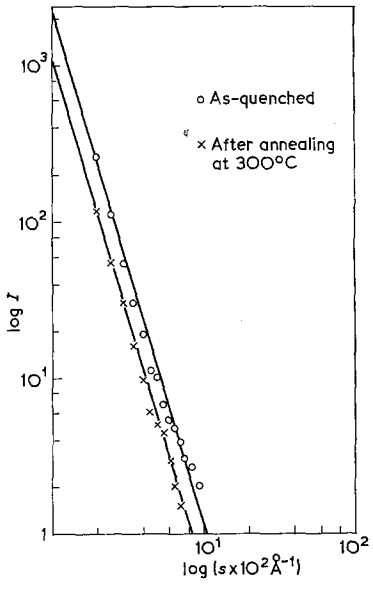

Figure 2 Log I versus log s for Al–3.6 at. % Ni.

radiation diminished, because although the volume of some agglomerates increased, their specific surface decreased. The intensities of scattered radiation measured on samples annealed at 300°C agreed better with the s^{-4} curve than the corresponding intensities measured on as-quenched samples, as can be seen in Fig. 2. This better agreement may be explained by the existence of a more distinct boundary between the matrix and the agglomerates. At annealing temperatures above 300°C the lines of Al_3Ni precipitates appeared at higher diffraction angles.

Analysis of the scattering curves indicated that the Al–3.6 at. % Ni alloy (in our samples about 20 μm thick) obtained by the splat-cooling technique is not a real solid solution, but that agglomerates of Ni atoms exist already in the as-quenched alloy. These agglomerates grow in the course of the annealing process.

After quenching from the melt thin areas of Al–3.6 at. % Ni were examined in a Philips EM 300 electron microscope. In certain parts of these samples clusteres with diameters of about 50 Å were found (Fig. 3a), but places with no clusters were also detected, as visible in Fig. 3b. After annealing for 1 h at about 150°C, clusters appeared in all examined positions of the sample, even in those positions where they could not be detected in as-quenched samples, as visible in Fig. 3c. With further annealing at temperatures above 150°C these clusters transform into semi-coherent platelets of η phase [4]. Around each plate there exists a distortion field, visible for example at points A in Fig. 3d. The appearance of Al_3Ni precipitates accompanied by a gradual disappearance of the lattice distortions, as detected in the electron-microscope at temperatures of about 300°C, is illustrated in Fig. 3e. Al_3Ni lines appeared in the X-ray diagrams at about the same temperature.

Microhardness measurements on Al–3.6 at. % Ni alloys rapidly quenched from the melt, after annealing for 10 min at temperatures of up to 500°C, were made by Tonejc *et al.* [4]. They stated that the initial hardness of as-quenched flakes of Al–3.6 at. % Ni alloys containing only solid solution was about five times the hardness of rapidly quenched pure aluminium. The increase in hardness during annealing at temperatures of up to about 100°C, without the lattice parameter spacings changing, indicated that some process occurred which is characteristic for precipitation strengthening. As on corresponding Debye-Scherrer diagrams no lines corresponding to a new phase were detected, it was supposed that the increase in hardness was due to coherent precipitates. At annealing temperatures exceeding 150°C hardness decreased, and at 300°C lines of stable precipitates appeared.

Microstrains and their changes during annealing in Al–3.6 at. % Ni alloys were also studied [6]. Changes in intensity $\triangle I$ (for $s = 2 \times 10^{-2}$ Å^{-1}) during annealing, with respect to the as-quenched sample, and the corresponding variation in microhardness $\triangle H$ obtained by Tonejc *et al.* [4], and in microstrains [6] obtained by Kirin *et al.* are presented in Fig. 4. It is evident that all three curves reach their maximum at about the same annealing temperature, and that changes of microhardness $\triangle H$ – and in some measure the changes of microstrains $\Delta\epsilon$ – accompany changes of intensity $\triangle I$.

4.2 Al–0.26 at. % Sn samples quenched from the melt

X-ray scattering on the Al–0.26 at. % Sn solid solution, provided that it is homogenous, would be constant with the value of *cca* 3.4 electrons per atom in the angular domain of our measurements ($s = 2 \times 10^{-2}$ to 9×10^{-2} Å^{-1}). The scattering intensities measured on the Al–0.26 at. % Sn alloy, after subtracting the scattering obtained on the pure aluminium sample, are given in Table II. The intensities of the as-quenched sample and

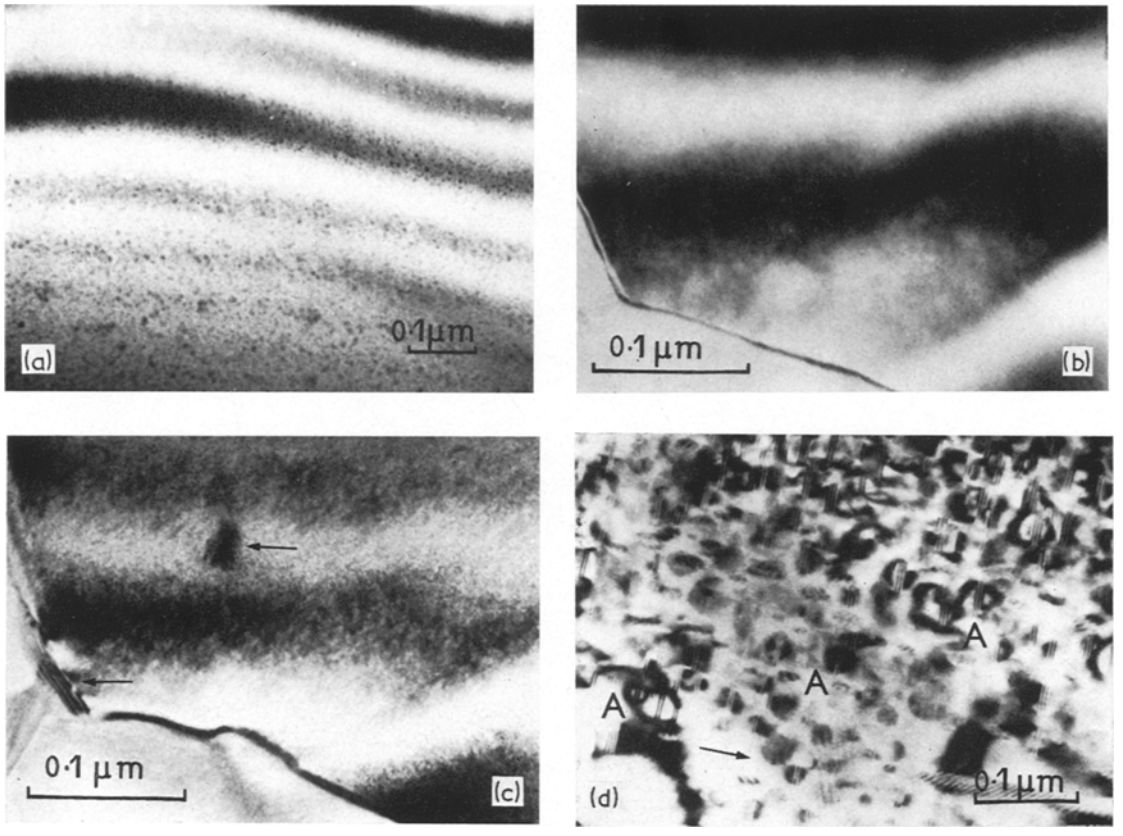

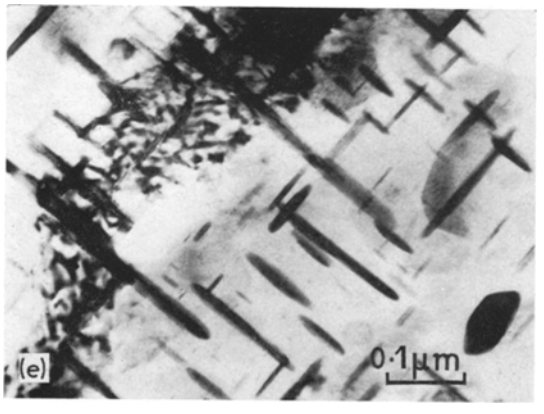

Figure 3 (a) Electron micrograph of an as-quenched Al–3.6 at. % Ni alloy showing Ni-rich clusters. The size of clusters diminish from the bottom to the top of the picture, as the foil thickness decreases. (b) Electron micrograph of an as-quenched Al–3.6 at. % Ni alloy. In this figure one of the thinnest parts of specimen is shown. No agglomerates of Ni atoms are visible immediately after quenching. (c) Same as (b) but aged for 1 h at 150°C in the microscope using hot stage. Ni-rich clusters with average diameter of about 15 Å are uniformly dispersed in the interior of the grain. Particles of intermetallic phase are shown by arrows. (d) Electron micrograph of the same alloy aged to produce platelets of the metastable η-phase. Arrow indicates the g_{200} diffraction vector of strongly excited matrix reflection. Characteristic strain field contrast around platelike precipitates is clearly seen at A. (e) Electron micrograph of the same alloy aged to produce incoherent platelike precipitates of stable Al_3Ni phase lying in the {100} matrix planes. The beam direction is close to matrix [100].

the intensities after isochronal annealing at 140 and 300°C are presented in Fig. 5. These curves are similar to the curves obtained with Al–3.6 at. % Ni samples. Although the difference in atomic scattering factors in the Al–Sn system is higher than in the Al–Ni system, the small concentration of Sn atoms is the reason for the smaller intensity of scattering in Al–0.26 at. % Sn in comparison with the Al–3.6 at. % Ni sample.

The scattering obtained on the sample Al–0.26 at. % Sn immediately after quenching from the melt and after annealing for 10 min at 140°C and 300°C is represented in the log I – log s diagram in Fig. 6. The measured points lie on the approximately straight lines with the

TABLE II

$s \times 10^2$ Å^{-1}	$I(s)$ electrons per atom						
	20°C	50°C	100°C	140°C	200°C	300°C	400°C
2.0	109.1	45.3	35.6	57.5	55.1	18.8	16.8
2.5	47.7	23.1	23.8	28.3	25.0	11.0	10.3
3.0	27.0	13.5	13.8	15.9	12.1	6.6	6.5
3.5	14.4	6.8	7.1	9.6	7.6	3.8	4.4
4.0	8.8	4.2	4.6	5.9	4.8	2.7	2.6
4.5	5.7	1.9	2.9	4.0	2.2	1.6	1.6
5.0	4.7	1.7	1.2	2.6	1.6	0.8	0.5
5.5	3.6	0.6	1.1	2.2	1.4	0.4	0.4
6.0	3.4	0.5	0.7	1.5	0.9	0.7	0.1
6.5	2.9	0.1	0.7	0.8	0.3	0.4	0.1
7.0	2.6	0.2	0.5	0.8	0.3	0.3	0.3
7.5	2.2	0.5	0.4	0.5	0.1	0.0	0.0
8.5	1.7	0.2	0.5	0.4	0.1	0.0	0.1
9.5	1.5	0.0	0.0	0.3	0.2	0.0	0.0

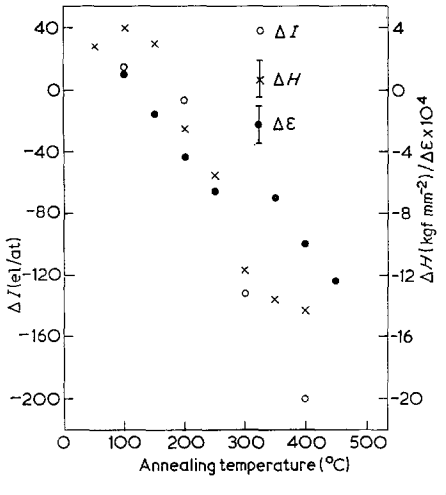

Figure 4 Changes in intensity ΔI (for $s = 2 \times 10^{-2}$ Å^{-1}) during annealing, with respect to the as-quenched sample and the corresponding variations in microhardness ΔH and microstrains $\Delta\epsilon$.

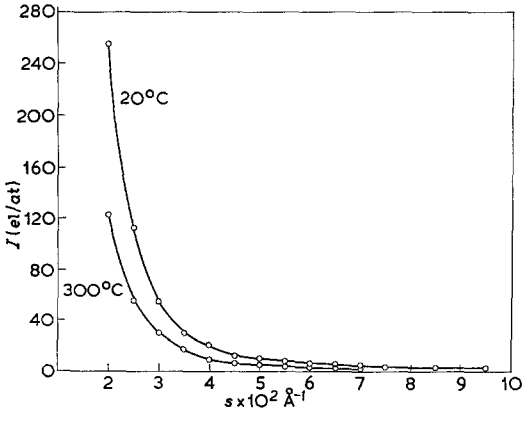

Figure 5 The intensities of scattering for as-quenched Al–0.26 at. % Sn sample before and after isochronal annealing for 10 min at 140°C and 300°C.

slope − 4, and therefore we interpreted the scattering applying Porod's law, which makes it possible to determine the internal surface and, in favourable cases, the size of the particles. Supposing that the particles are spherical and that their structure is the same as the structure of β–Sn, we calculated the dimensions of the clusters in the same way as described in the case of the Al–3.6 at. % Ni system. The calculations gave a mean radius of clusters of 50 Å in as-quenched samples, after annealing at 140°C 95 Å, and after annealing at 300°C a mean radius of 240 Å.

Electron-microscopic examinations made on the margins of the quenched foils, where areas suitable for electron-microscopic examinations are situated, also revealed the precipitates of a new phase in some splat-cooled samples. After annealing for ten minutes at 150°C, in areas where in as-quenched samples only solid solution was present, precipitates of the β–Sn phase were observed. This is illustrated in Fig. 7a and b. The diameters of the clusters varied in this case from 25 to 50 Å.

The changes in intensity of scattered X-rays $\triangle I$ (for $s = 2{\cdot}5 \times 10^{-2}$ Å^{-1}) and the variation in $\triangle H$ during annealing are represented in Fig. 8. The course of these points is similar to that of analogous points obtained on the Al–3.6 at. % Ni system represented in Fig. 4. However, there

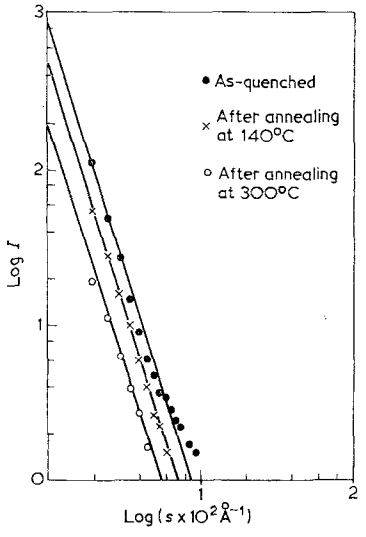

Figure 6 The scattering obtained for Al–0.26 at. % Sn immediately after quenching from the melt and after annealing for 10 min at 140°C and 300°C shown in a log I – log s diagram.

is a difference in the course of the $\triangle I$ and $\triangle H$ lines in the earliest stages of annealing. In the Al–0.26 at. % Sn system the $\triangle I$ and $\triangle H$ curves reached maximum value at about 100°C, without a tendency of decreasing at the beginning of annealing.

5. Final discussion and conclusions

Al–3.6 at. % Ni and Al–0.26 at. % Sn alloys examined by means of small angle X-ray scattering always show variable dimension heterogeneities. In as-quenched samples of these alloys, examined in an electron microscope, areas where only solid solution was present were observed, while clusters appeared later on a certain stage of annealing.

It should be noted that the calculations of the dimensions of clusters given in this paper were made by rough approximations and should therefore be considered merely as an attempt to obtain a quantitative representation of the process of clustering during annealing. Moreover, the samples used in the X-ray examinations were not ideal with respect to solid solubility. We chose samples from 10 to 20 μm thick, as a compromise between the optimal thickness for X-ray scattering (65.3 μm for Al–3.6 at. % Ni and 72.8 μm for Al–0.26 at. % Sn) and samples thinner than 10 μm, which may be considered as more effectively quenched

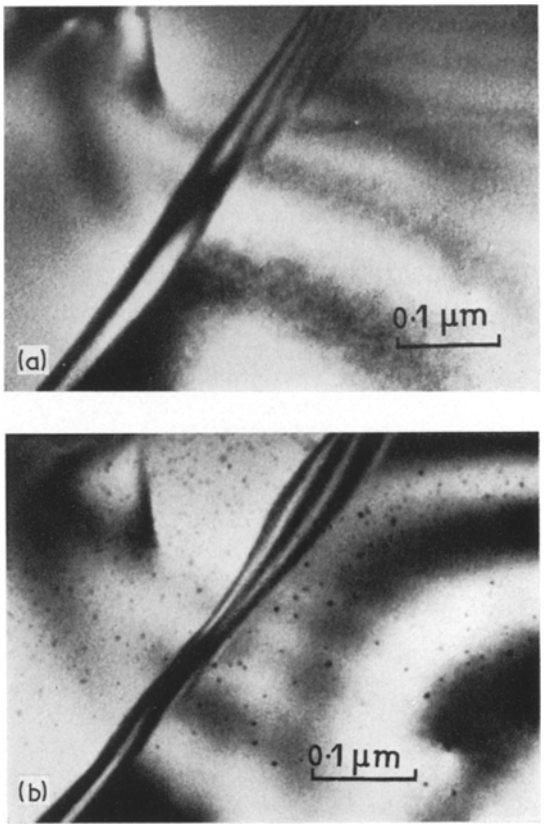

Figure 7 (a) Electron micrograph of an as-quenched Al–0.26 at. % Sn alloy. No Sn-rich clusters are visible in the adjacent grains immediately after quenching. (b) Electron micrograph of the same area as in (a) after annealing for 10 min at 150°C in the microscope using hot stage. Circular black dots of 20 Å to 50 Å in diameter are clearly visible. They represent spherical particles of β–Sn, as determined from the corresponding electron diffractogram.

[18]. Electron microscopic measurements were made on thinner, and for 100 keV electrons transparent, about 1 μm thick domains on the margin of the samples. A certain difference between the results of X-ray small-angle scattering and the electron-microscopic examinations may be expected, because the examinations were performed on samples containing different, more or less imperfect, solid solutions.

The process of approaching equilibrium in these solid solutions is not monotonous, but during annealing passes through metastable states which affect the mechanical properties of the samples.

Maxima in the $\triangle I$ curves of the Al–3.6 at.% Ni system represented in Fig. 4 and in Fig. 8 might

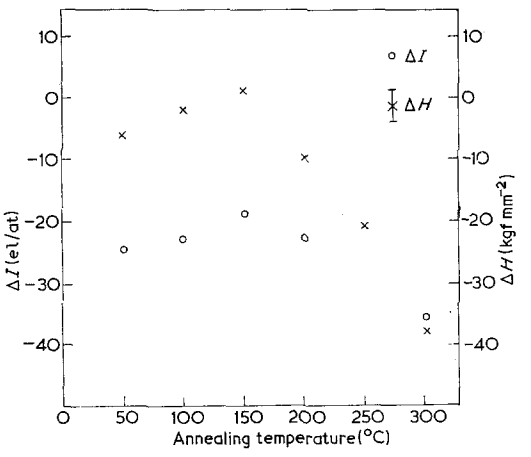

Figure 8 Changes in intensity ΔI for $s = 2 \times 10^{-2}$ Å^{-1} during annealing, with respect to as-quenched Al-0.26 at.% Sn sample and the corresponding variations in microhardness ΔH.

in principle be associated with any of the following changes in the specimens during annealing:

(a) modification of the intensity of the double Bragg reflection

(b) establishment of the short-range order

(c) formation of stacking faults

(d) formation of clusters due to the segregation of solute atoms.

Alternative (a) can be excluded, because according to the theory of the double Bragg reflection [13] the intensity of scattering caused by double reflection is proportional to the inverse square of the mean subgrain diameter. The growth of subgrains during the annealing process should produce a steady decrease of the small-angle scattering. Thus the maxima of intensity which appear in Fig. 4 and Fig. 8 could not be explained by the double Bragg reflection.

Alternative (b) is also improbable since an increase of order will decrease the Laue scattering [19]. In the case of the short range order, the order parameters α_m are negative, and thus the Laue scattering given by Equation 6 should be inferior in comparison with the scattering of a disordered alloy.

Alternative (c) was examined in detail by Kirin *et al.* [6] who studied X-ray line broadening in splat-cooled aluminium-nickel and aluminium-tin solid solutions. They found that the main source of the line broadening in these systems are microstrains and that the deformation fault probability was insignificant. No faulting in these systems could be detected in the electron microscope.

All three alternatives (a), (b) and (c) may thus be eliminated from further considerations. Our conclusion is that the maxima in $\triangle I$ curves are connected with the evolution of clusters of solute atoms at a certain stage of annealing. Thus the increase of scattered X-rays intensity at $s = 2 \times 10^{-2}$ Å^{-1} in the Al–3.6 at. % Ni system, resulting from heat treatment at 100°C, was observed, as represented in Fig. 4. By analogous heat treatment on the heating stage of the electron microscope at about the same temperature the formation of agglomerates of Ni atoms was observed. These microprecipitates are surrounded by a strained region of the matrix, as illustrated in Fig. 3d. In that stage of annealing, microhardness and microstrain also show a small increase. With longer annealing new phases appeared while $\triangle I$, $\triangle H$ and $\triangle \epsilon$ decreased as the system approached equilibrium.

In the Al–0.26 at. % Sn system a similar behaviour of $\triangle I$ and $\triangle H$ in the annealing process was obtained as in the Al–3.6 at. % Ni system, as shown in Fig. 8. Measurements of microstrain variations on that system were not made and thus could not be presented in Fig. 8. Clusters of Sn atoms at the stage of annealing at 150°C were also detected in the electron microscope, as visible in Fig. 7b. The minima in the $\triangle I$ and $\triangle H$ curves at an annealing temperature of 50°C might be explained by the relaxation of lattice distortions introduced by splat-cooling. A slow decrease in microhardness with increasing annealing temperature was also detected in isochronally annealed quenched flakes of pure aluminium. Probably this process also exists in Al–3.6 at. % Ni; however in that system the lattice distortion caused by dissolved Ni atoms is dominant, due to a high concentration of Ni atoms, and thus the minima in $\triangle I$ and $\triangle H$ curves are not present.

The work of Cahn and Davies [20] may also be relevant to the results reported here. Using the X-ray technique, these authors have investigated the process of segregations of solute in a Cu–Al alloy and found that the increased small-angle scattering, resulting from heat-treatment at 150 to 250°C, is due to a segregation of solute to the stacking faults. They too found that the hardness increase at each stage of annealing was proportional to the intensity of the X-ray scattering.

References

1. POL DUWEZ and R. H. WILLENS, *Trans. Met. Soc. AIME* **227** (1963) 362.
2. A. FONTAINE, *Fizika* **2** Suppl. 2 (1970) 23.
3. E. DARTYGE, M. LAMBERT, G. LEROUX and A. M. LEVELUT, *Acta Met.* **20** (1972) 233.
4. A. TONEJC, D. ROČAK and A. BONEFAČIĆ, *Acta Met.* **19** (1971) 311.
5. A. KIRIN and A. BONEFAČIĆ, *Scripta Met.* **4** (1970) 525.
6. A. KIRIN and A. BONEFAČIĆ, *J. Phys. F*, in print.
7. R. HEZEL and S. STEEB, *Z. Naturforsch.* **25** (1970) 1085.
8. A. TONEJC and A. BONEFAČIĆ, *J. Appl. Phys.* **40** (1969) 419.
9. A. M. LEVELUT and A. GUINIER, "Small-Angle Scattering of X-rays", (edited by H. Brumberger,) (Gordon and Breach, New York, 1967) p. 351.
10. A. M. LEVELUT, Ph.D. Thesis, Université de Paris, 1968.
11. C. B. WALKER, *Phys. Rev.* **103** (1956) 547.
12. *Idem, ibid* **103** (1956) 558.
13. B. E. WARREN, *Acta Cryst.* **12** (1959) 837.
14. A. GUINIER, "Théorie et technique de la radiocristallographie" (Dunoa, Paris, 1964) p. 574.
15. *Idem, ibid*, p. 578.
16. *Idem, ibid*, p. 637.
17. G. POROD, *Kolloid- Z.* **124** (1951) 83.
18. J. N. GRANT, *Fizika* **2** Suppl. 2 (1970) 16.
19. V. I. IVERONOVA and A. A. KACNELJSON, *Fiz. Met. i Metall.* **24** (1967) 966.
20. R. W. CAHN and R. G. DAVIES, *Phil. Mag.* **5** (1960) 1119.

Received 24 June and accepted 27 August 1974.